

Theory of resonantly enhanced photo-induced superconductivity

Christian J. Eckhardt,^{1,2} Sambuddha Chattopadhyay,³ Dante M. Kennes,^{1,2}
Eugene A. Demler,⁴ Michael A. Sentef,^{5,2} and Marios H. Michael²

¹*Institut für Theorie der Statistischen Physik, RWTH Aachen University and
JARA-Fundamentals of Future Information Technology, 52056 Aachen, Germany*

²*Max Planck Institute for the Structure and Dynamics of Matter, Center for
Free-Electron Laser Science (CFEL), Luruper Chaussee 149, 22761 Hamburg, Germany*

³*Lyman Laboratory, Department of Physics, Harvard University, Cambridge, MA 02138, USA*

⁴*Institute for Theoretical Physics, ETH Zürich, 8093 Zürich, Switzerland*

⁵*H H Wills Physics Laboratory, University of Bristol, Bristol BS8 1TL, United Kingdom*

(Dated: March 7, 2023)

Optical driving of materials has emerged as a promising tool to control their macroscopic properties. In this work we present a microscopic mechanism for efficiently photo-inducing superconductivity. We investigate an attractive electron-electron interaction mediated by a boson that couples to an electronic transition between two bands separated by a band gap. While this attraction is small in equilibrium, we find that it can be increased by several orders of magnitude when the bosons are driven into a nonthermal state. Moreover, not only is the induced attraction enhanced when the bosons are driven, but this enhancement is further amplified when the boson is near-resonant to the electronic interband excitation energy, making this mechanism a potentially ideal candidate for efficient photo-induced superconductivity. We first use exact diagonalisation calculations of a two-site model to prove that pairing is indeed resonantly enhanced out-of equilibrium. We then investigate the potential of this mechanism to increase the superconducting transition temperature, and find by investigating the gap equation that pairing is resonantly amplified when the bosons are in a nonthermal state. We argue that our proposed mechanism provides a simple prescription for designing new platforms that enable photo-induced superconductivity at significant temperatures and moderate driving strengths, and estimate a transition temperature $T_c \approx 5\text{K}$ for a SrTiO_3 – graphene heterostructure.

INTRODUCTION

Engineering materials properties or even effecting new phases of matter by irradiating samples with light is one of the most tantalizing prospects of modern condensed matter physics.^{1–3} Experimentally, laser light has been shown to be a versatile tool in a variety of systems capable of inducing ferro-electricity^{4,5} or switching between charge density wave states^{6–8}. Arguably the most exciting prospect is to use light to engineer superconducting-like behavior up to room temperature. Experimentally, putative evidence for creating superconducting-like states in K_3C_{60} ^{9–11} and certain organic compounds¹² through laser driving in the THz range have made this prospect all the more likely.

Theoretically, progress in understanding photo-driven states has blossomed, with a variety of proposals attempting to understand the phenomenology of photo-induced superconductivity^{13–31}. However, a simple microscopic and experimentally realistic mechanism that predicts efficiently photo-created superconductivity, able to direct future experimental explorations, remains elusive. In this paper, we explore such a mechanism based on a boson—such as phonon, plasmon or surface plasmon—locally coupling to an inter-band electronic transition as shown in Figure 1(a). We demonstrate that these ingredients lead to a boson-mediated electron attraction that not only increases during pumping but is

further resonantly amplified when the boson frequency is close to the inter-band transition energy—potentially enhancing the efficiency of the light-induced state by orders of magnitude.

Interestingly, the importance of a local interband-phonon coupling has been discussed before in the context of equilibrium superconductivity in doped SrTiO_3 .^{32–34} The goal of this paper is to spotlight the potentially transformational implications for photo-induced superconductivity not discussed in the literature before, and then provide a simple prescription for finding new non-thermal settings where superconductivity can be efficiently created.

In the following, we present a minimal model and investigate its properties with a focus on driving-induced superconductivity. To this end, we first demonstrate that resonantly enhanced electron attraction is induced in the boson-driven case by performing exact diagonalisation calculations on a two-site model. We then explore the consequences of this mechanism to superconductivity of extended systems by deriving the gap equation using the Matsubara formalism. Consistent with the exact diagonalisation results, we find that the resonance is absent in equilibrium, but the boson-mediated electron-electron attraction can be resonantly enhanced by several orders of magnitude when the bosons are driven into a nonthermal state.

Finally, we propose two-dimensional materials cou-

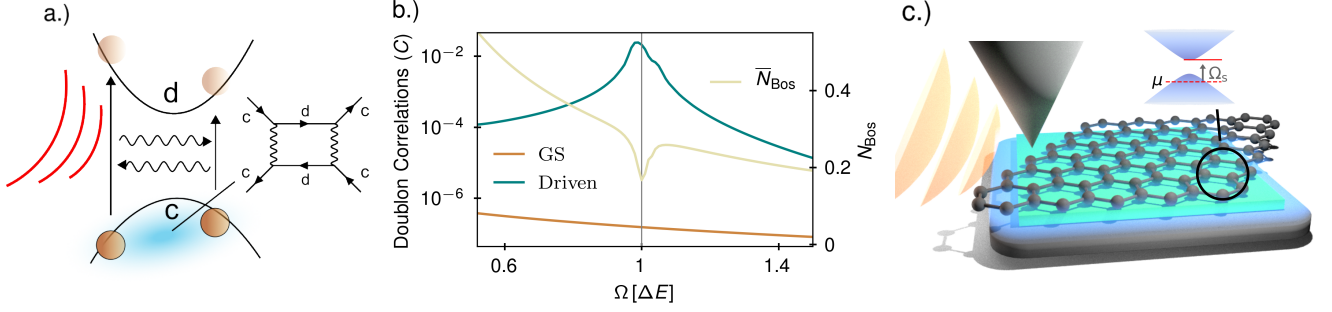


FIG. 1. **a.)** A boson coupling to an electronic inter-band transition can induce an effective electron-electron attraction stemming from virtual processes that involve the exchange of two bosons. Away from the groundstate, when real bosons populate the mode, for example when driving the system, this attraction may be resonantly enhanced when tuning the boson frequency close to the transition energy. **b.)** Exact diagonalisation results for the proposed mechanism. Local doublon correlation C (Eq. (6)) in the two-site model given by Eq. (1) as a function of bosonic frequency Ω in units of the level separation ΔE . The value in the groundstate (orange line, left axis) shows no resonant behaviour, but for coherently driven bosons (blue line, left axis) the time-averaged doublon correlations show a sharp increase when $\Omega \approx \Delta$. On resonance the time-averaged boson number \bar{N}_{bos} (yellow line, right axis) has a dip since carriers are excited into the upper level, detrimental to pairing. The level coupling and the hopping have been set to $g = t = 0.01\Delta E$. **c.)** Illustration of the hetero structure we propose. Graphene (black) aligned with hBN (green) is placed on top of bulk SrTiO₃ (black bottom layer). Surface plasmon polaritons (light blue shade) on the surface of SrTiO₃ couple the two graphene bands that develop a gap due to the alignment with hBN. The chemical potential μ is set such that the surface plasma frequency can be close to resonance between the fermi level in the lower band and the bottom of the upper as shown in the inset. The surface plasmons can be driven by irradiating a tip (orange waves onto tip) and utilizing its near field.

pled to surface plasma modes of a substrate as an ideal platform to engineer photo-induced superconductivity at temperatures much higher than their equilibrium T_c . As a simple and easily accessible example, we explore a heterostructure consisting of graphene aligned with hexagonal boron nitride (hBN)^{35–38} on top of the surface of SrTiO₃. Graphene aligned with hBN hosts two electronic bands with a small gap, while the SrTiO₃ surface provides surface plasmon polaritons at a similar frequency as the gap. We estimate that photo-induced pairing in graphene could be induced up to a critical temperature of around 5K.

RESULTS

Mechanism for induced electron-electron attraction

We investigate a lattice model of electrons in which each site has two orbitals that are coupled locally via a boson

$$\begin{aligned}
 H^{\text{loc}} &= H_0 + H_{\text{int}} \\
 H_0 &= \sum_{\sigma,j} \frac{\Delta E}{2} \left(d_{j,\sigma}^\dagger d_{j,\sigma} - c_{j,\sigma}^\dagger c_{j,\sigma} \right) + \Omega b_j^\dagger b_j \\
 H_{\text{int}} &= g \sum_j \left(b_j^\dagger + b_j \right) \sum_\sigma \left(d_{j,\sigma}^\dagger c_{j,\sigma} + c_{j,\sigma}^\dagger d_{j,\sigma} \right).
 \end{aligned} \tag{1}$$

Here $c_{\sigma,j}$ and $c_{\sigma,j}^\dagger$ are annihilation and creation operators of electrons in the lower level with spin σ at site j while $d_{\sigma,j}$ and $d_{\sigma,j}^\dagger$ are annihilation and creation operators of electrons in the upper level that is separated from the

lower one by the energy gap ΔE . b_j^\dagger and b_j are bosonic creators and annihilators of the bosonic mode at site j that has eigenfrequency Ω and couples the two electronic levels with coupling strength g .

We perform a Schrieffer-Wolf transformation of the Hamiltonian in Eq. (1) to eliminate the coupling to leading order in g . As shown in Methods section we find

$$\begin{aligned}
 H^{\text{SW}} &= H_0 \\
 &- g^2 \frac{\Delta E}{(\Delta E)^2 - \Omega^2} \sum_j \left(b_j^\dagger + b_j \right)^2 \sum_\sigma \left(d_{j,\sigma}^\dagger d_{j,\sigma} - c_{j,\sigma}^\dagger c_{j,\sigma} \right) \\
 &- g^2 \frac{\Omega}{(\Delta E)^2 - \Omega^2} \left(\sum_{j,\sigma} d_{j,\sigma}^\dagger c_{j,\sigma} + c_{j,\sigma}^\dagger d_{j,\sigma} \right)^2.
 \end{aligned} \tag{2}$$

The second term constitutes an electronic density coupled to the squared boson displacement.²⁴ In Ref. 13 such an interaction was considered on symmetry grounds and it was shown that it gives rise to a boson-number dependent attraction :

$$H_{\text{att}} = -4g^4 \frac{\Delta E^2}{\Omega ((\Delta E)^2 - \Omega^2)^2} \sum_j \left(b_j^\dagger b_j c_{j,\uparrow}^\dagger c_{j,\downarrow}^\dagger c_{j,\downarrow} c_{j,\uparrow} \right). \tag{3}$$

Here we show how such a term arises naturally from a microscopic model. The prefactor $(\Delta E^2 - \Omega^2)^{-2}$ suggests that this attraction may even be resonantly enhanced when tuning the bosonic frequency close to the level transition $\Omega \approx \Delta E$. Despite this intriguing result, to study the correct attraction close to the resonance both the

bosonic part and the electronic part involving the upper band in equation 2 needs to be taken into account consistently to order g^4 . These effects are taken into account in the following paragraphs by performing ground-state perturbation theory and exact diagonalisation for the two-site model.

Groundstate attraction– In this part we treat the full model using ground-state perturbation theory. We show that in this case, a resonant enhancement of the induced electron-electron interaction as indicated by Eq. (3) is indeed absent. We focus on the most simple two-site version, $j \in \{1, 2\}$, of the model in equation (1) and consider a half filled lower level with two electrons in the system overall. At vanishing coupling $g = 0$ the groundstate of the system with no bosons is degenerate between two unpaired electrons on different sites and a singlet on the same site. In other words, the energy of one doubly occupied site and an empty site $E_{\uparrow\downarrow,-}^{\text{GS}}$ matches that of two singly occupied sites $E_{\uparrow\downarrow}^{\text{GS}}$. Upon turning on the coupling $g > 0$ this degeneracy is lifted: The state with a doubly occupied site obtains a slightly lower energy than two singly occupied sites. To leading order in the coupling g the energy difference is

$$E_{\uparrow\downarrow,-}^{\text{GS}} - E_{\uparrow\downarrow}^{\text{GS}} = -2g^4 \frac{\Omega + 2\Delta E}{(\Delta E)\Omega(\Delta E + \Omega)^2}. \quad (4)$$

We interpret this energy as an attractive interaction between the two electrons. Consistent with Eq. (3) it is fourth order in the coupling g . However, Eq. (4) shows no special features when $\Delta E \approx \Omega$ particular to resonant enhancement of the attraction.

Photo-induced attraction– To explore the induced attraction away from the groundstate, we perform exact diagonalisation calculations on the two-site model of equation (1) including a small hopping term parametrized by the hopping amplitude t

$$H = H^{\text{loc}} - t \sum_{j,\sigma} \left(c_{j+1,\sigma}^\dagger c_{j,\sigma} + d_{j+1,\sigma}^\dagger d_{j,\sigma} \right) + \text{h.c.} \quad (5)$$

First we compute the lower level doublon correlations in the groundstate,

$$C = \sum_j \langle n_{j,\uparrow}^c n_{j,\downarrow}^c \rangle - \langle n_{j,\uparrow}^c \rangle \langle n_{j,\downarrow}^c \rangle, \quad (6)$$

as an indicator of an induced electron-electron interaction. The result is shown in Fig. 1(b). Consistent with our perturbative analysis in equation (4), in the groundstate, we find positive correlations indicating an effective attraction that increases towards lower frequencies but show no specific features at $\Delta E \approx \Omega$.

To analyse the out of equilibrium case, we coherently drive the bosons and compute the time-averaged density correlations Eq. (6) as well as the time-averaged boson number $\int_{t_0}^{t_1} dt \langle b_j^\dagger b_j \rangle(t) = \bar{N}_{\text{bos}}$, where t_0 is a time

shortly after the driving pulse and t_1 a later time after many driving periods. Details on how we perform the time evolution can be found in the methods section. We find an overall amplification of the electron-electron attraction compared to the equilibrium result. Moreover, while in equilibrium no enhancement of the interaction close to resonance $\Omega \approx \Delta E$ was found, such an enhancement can indeed be accessed out of equilibrium as can be seen in Fig. 1(b). The resonance is also evident in the time-averaged number of bosons, which has a dip indicating that electrons are being excited into the upper level by absorbing bosons.

Dynamic gap equation– In this part we investigate how the mechanism described above might give rise to superconductivity in real materials. We consider a two-band system with band dispersions $\varepsilon_c(k)$ and $\varepsilon_d(k)$, where $\varepsilon_d(k) > \varepsilon_c(k)$ for all quasi-momenta k throughout the Brillouin zone. We write the uncoupled Hamiltonian of this system as

$$H_0 = \sum_{\vec{k},\sigma} \left(\varepsilon_c(\vec{k}) c_{\vec{k},\sigma}^\dagger c_{\vec{k},\sigma} + \varepsilon_d(k) d_{\vec{k},\sigma}^\dagger d_{\vec{k},\sigma} \right) \quad (7)$$

where $c_{k,\sigma}$ annihilates; $c_{k,\sigma}^\dagger$ creates an electron with spin σ and quasi-momentum k in the lower band while $d_{k,\sigma}$ annihilates; $d_{k,\sigma}^\dagger$ creates an electron with spin σ and quasi-momentum k in the upper band. We couple both bands linearly through a boson

$$H = H_0 + H_{\text{int}} + \sum_q \Omega(q) b_q^\dagger b_q, \\ H_{\text{int}} = \sum_q g(q) \left(b_{-q}^\dagger + b_q \right) \sum_{k,\sigma} \left(c_{k+q,\sigma}^\dagger d_{k,\sigma} + d_{k+q,\sigma}^\dagger c_{k,\sigma} \right), \quad (8)$$

where b_q annihilates; b_q^\dagger creates a boson with momentum q and frequency $\Omega(q)$ while $g(q)$ parametrizes the coupling strength to the electrons. We integrate out the bosons exactly using the Matsubara path-integral approach yielding a dynamic electron-electron interaction. The dependence of this interaction on the state of the bosons is encoded in the frequency structure of the interaction. We then perform a saddle point approximation to compute the intra-band pairing fields $\Delta_c = \langle \psi_{k,\uparrow,c} \psi_{k,\downarrow,c} \rangle$ and $\Delta_d = \langle \psi_{k,\uparrow,d} \psi_{k,\downarrow,d} \rangle$, and we arrive at two coupled gap equations for Δ_c and Δ_d , shown diagrammatically in Fig. 2(a) :

$$\Delta_c(k, \omega) = \frac{1}{N\beta} \sum_{\vec{k}', \omega'} \frac{g(k-k')g(k'-k)\Omega(k-k')}{(\omega - \omega')^2 + \Omega(k-k')^2} \quad (9)$$

$$\frac{\Delta_d(k', \omega')}{2E_c(\vec{k}')} \left(\frac{1}{i\omega' - E_c(k')} - \frac{1}{i\omega' + E_c(k')} \right),$$

$$\Delta_d(k, \omega) = \frac{1}{N\beta} \sum_{k', \omega'} \frac{g(k-k')g(k'-k)\Omega(k-k')}{(\omega - \omega')^2 + \Omega(k-k')^2} \quad (10)$$

$$\frac{\Delta_c(k', \omega')}{2E_d(k')} \left(\frac{1}{i\omega' - E_d(k')} - \frac{1}{i\omega' + E_d(k')} \right),$$

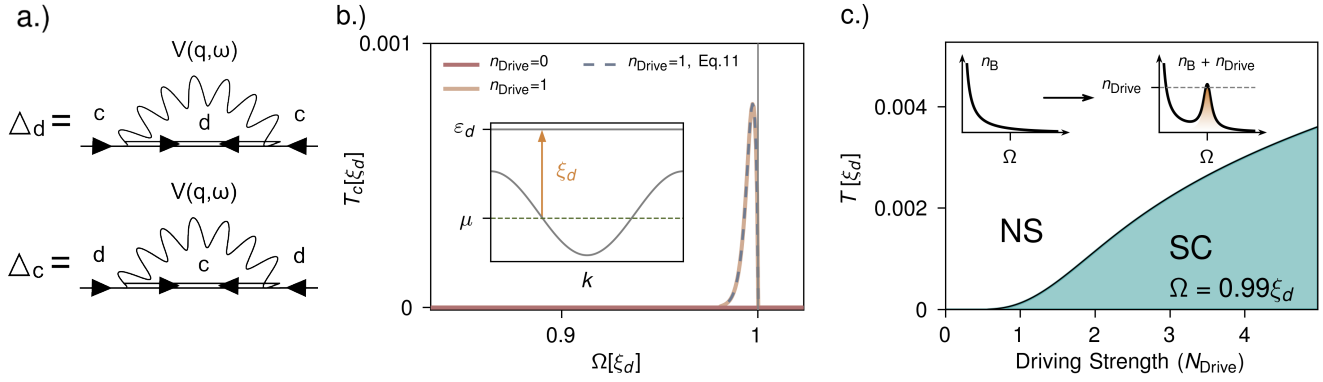


FIG. 2. **a.)** Feynman diagrams for the coupled gap equations Eq. (9) and (10). **b.)** Critical temperature T_c as a function of frequency Ω for the sawtooth chain. The dispersion of the sawtooth chain is shown in the inset with $\xi_d = \varepsilon_d - \mu$ indicated. In thermal equilibrium (red line) no significant T_c is found while driving the bosons increasing their occupation by N_{Drive} Eq. (15) yields a resonantly enhanced T_c for $\Omega \lesssim \xi_d$ where both the full expression Eq. (26) (yellow line) and the approximate expression Eq. (11) (blue dashed line) agree. **c.)** Nonequilibrium phase diagram as function of temperature T and driving strength n_{Drive} (Eq. (15)) in units of ξ_d . At a critical driving strength the system changes from the normal state (NS) to a superconducting state (SC). The inset illustrates the non-thermal boson distribution we assume according to Eq. (15). The coupling g has been set to $g = 0.2\xi_d$ throughout while the chemical potential μ is set such that $\xi_d = 3t$, where t is the nearest neighbour hopping.

where we have introduced the Bogoliubov dispersion $E_{c/d}(k) = \sqrt{\xi_{c/d}(k)^2 + \Delta_{c/d}(k)^2}$ and $\xi_{c/d} = \varepsilon_{c/d} - \mu$.

In order to estimate T_c we assume a local coupling $g(q) = g$ and a flat bosonic dispersion $\Omega(q) = \Omega$. We next insert the equation for Δ_d into that of Δ_c arriving at a single self-consistent gap equation for Δ_c . We find $\Delta_c(\omega)$ to only have a weak frequency dependence for $\omega < \Omega$ and therefore neglect this dependence for an estimate of T_c . In this way, we can evaluate all Matsubara sums by analytically continuing to real frequencies and introducing bosonic and fermionic occupation functions. The details of the calculation and the full gap equation

are given in the methods section and the supplementary material.

Similar to the standard BCS approach for superconductivity in a single band, we only keep the most divergent terms contributing to the gap equation. We identify two small parameters close to the Fermi surface when $|\xi_c| \ll |\xi_d| \approx \Omega$, namely the detuning between the upper band and the phonon frequency, $\frac{d_d}{\Omega} = \frac{\xi_d - \Omega}{\Omega}$, and the dispersion relation of the lower band, $\frac{|\xi_c|}{\Omega}$, and expand the gap equation to leading and next-to-leading order in these parameters. In this situation T_c can be determined from the following gap equation:

$$1 = L_{\text{BCS}}(T_c) + L_{\text{Non-BCS}}(T_c), \quad (11)$$

$$L_{\text{BCS}}(T_c) = \frac{g^4}{\Omega^3} \int_{-\Omega}^{\Omega} d\xi_c \nu(\xi_c) \int_{-\Omega}^{\Omega} d\xi_d \nu(\xi_d) (1 + n_B(\Omega) - n_F(|\xi_d|)) \frac{(1 - 2n_F(|\xi_c|))}{2|\xi_c|}, \quad (12)$$

$$L_{\text{Non-BCS}}(T_c) = \frac{g^4}{\Omega^2} \int_{-\Omega}^{\Omega} d\xi_c \nu(\xi_c) \int_{-\Omega}^{\Omega} d\xi_d \nu(\xi_d) (n_B(\Omega) + n_F(|\xi_d|)) \frac{(|\xi_d - \Omega|)(1 - 2n_F(|\xi_c|)) - |\xi_c|(1 - 2n_F(|\xi_d| - \Omega))}{|\xi_c|((|\xi_d| - \Omega)^2 - |\xi_c|^2)}. \quad (13)$$

Here n_B is the Bose distribution function, n_F is the Fermi distribution function, and $\nu(\xi)$ is the density of states at energy ξ . The integrals have a natural cut-off set by the bosonic frequency Ω , since the approximate expression for the gap equation is only valid within this energy window.

In equilibrium, the next to leading term in the gap

equation denoted as L_{BCS} , Eq. (12), corresponds to a BCS type gap equation. This gives rise to a T_c that precisely matches the one found in BCS theory with an effective local attraction of $U_{\text{eff}} = -\frac{g^4}{\Omega^3}$ computed from perturbation theory in the groundstate (see equation (4)).

The second term in equation (11), $L_{\text{Non-BCS}}$ Eq. (13), has no BCS analogue and diverges even more strongly as

$\frac{|\xi_d| - \Omega}{\Omega}, \frac{|\xi_c|}{\Omega} \rightarrow 0$. This is a manifestation of the resonance found in our model when the frequency matches the energetic distance from the Fermi level to the upper band. However, towards low temperatures $T \ll \Omega, |\xi_d|$, pairing from $L_{\text{Non-BCS}}$ is exponentially suppressed because it is proportional to either the number of phonons or the number of electrons in the upper band through the factor $n_b(\omega) + n_f(\xi_d)$. Therefore the resonance is absent in thermal equilibrium. We conjecture that, consistent with our analysis of the two-site model and Eq. (3), the leading order term, $L_{\text{Non-BCS}}$, in equation (11) can be activated out of equilibrium when the bosons are driven such that their distribution does not follow the Bose function.

We use the sawtooth chain^{39,40} to illustrate the interband phonon mechanism on a concrete example. This one-dimensional model consists of a dispersive lower band and a flat upper band:

$$\begin{aligned}\xi_c(k) &= -\sqrt{2}t(\cos(ka) + 1) - \mu \\ \xi_d(k) &= \sqrt{2}t - \mu.\end{aligned}\quad (14)$$

where a is the lattice constant, t the hopping between sites, and μ the chemical potential. The flat upper band in the sawtooth chain gives rise to a constant detuning, providing an idealised system to identify the resonance present in our model. We explore the possibility of using the nonequilibrium boson distribution as a resource by switching on the resonant contribution in the gap equation Eq. (11) through adjusting the equilibrium boson distribution to (cf. Fig. 2(c) for an illustration):

$$\langle b_q^\dagger b_q \rangle = n_B(\Omega) + n_{\text{Drive}}. \quad (15)$$

We compute T_c as a function of the boson frequency Ω and explore the resonance by tuning Ω across ξ_d . The result is shown in Fig. 2(b). In equilibrium we do not find a significant T_c for the coupling of $g = 0.2\xi_d$ and the selected frequencies. However, a significant T_c appears close to the resonant region as soon as we assume a nonthermal boson distribution according to Eq. (15). This behaviour is in agreement with the resonantly enhanced electron-electron interaction found in our exact diagonalisation calculations Fig. 1b. Both the full expression of the gap equation show in the methods section and the approximate expression in equation (11) match precisely close to the resonance. Unlike in the two-site model, in the extended system the driven-boson-induced interaction turns into repulsion for blue-detuned frequencies $\Omega \geq \xi_d$. Physically, we attribute this to the fact that the driven boson enables real transitions from the partially filled lower band to the empty upper band. Intriguingly, even though our semi-analytical treatment of the gap equations neglects a change of Fermi occupation functions, the mere possibility of real transitions is apparently reflected within Eq. (13), and it is detrimental to pairing. Importantly, an improved, but more involved treatment of the true nonequilibrium problem within the

Keldysh formalism is expected to exhibit the same qualitative behavior, since the excitation of real electronic quasiparticles above the gap will suppress pairing even further for a blue detuned boson frequency.

In order to summarize our findings for the driven sawtooth chain, we compute an out-of-equilibrium phase diagram as a function of temperature and driving strength (Fig. 2c), fixing Ω slightly below resonance, $\Omega = 0.99\xi_d$. While the system is in the normal state down to very low temperatures in equilibrium ($N_{\text{Drive}} = 0$) for $g = 0.2\xi_d$, populating the bosonic mode gives rise to a finite T_c .

Graphene-hBN-SrTiO₃ heterostructure.— We conclude by proposing an experimentally realizable platform for resonantly induced superconductivity, namely a heterostructure of graphene aligned with hBN placed on top of bulk SrTiO₃, as shown in Figure 1(c). Graphene aligned on hBN leads to a gap at the Dirac points of graphene, with size $\Delta E = 16\text{meV}$ ⁴¹, which will form the basis of our two-band electronic system. The bosonic mode key to our pairing model is provided by a low energy surface phonon polariton that exists in the quantum paraelectric SrTiO₃ and couples the two bands through their dipole moment.⁴² We compute this light-matter coupling using the mode functions obtained in Ref. 43 for the surface polaritons, and approximate the resulting coupling by a box function $g(q) = \tilde{g}\theta(|q| - \frac{1}{d})$, where d is the distance between the graphene and the SrTiO₃ surface which provides a natural cut-off for surface plasmon induced interactions. We assume an hBN thickness of 5nm, corresponding to approximately 15 atomic layers.⁴⁴ For a conservative estimate, we include the bare local Coulomb repulsion in graphene of $U = 9.3\text{eV}$. Dynamical suppression of the bare Coulomb repulsion due to high energy electrons via the Morel-Anderson renormalisation would enhance our results even further.⁴⁵ Our estimate is obtained by solving the full gap equation (26).

Without any driving the large Coulomb repulsion prevents any pairing. We find that when driving the system with $n_{\text{Drive}} = 1.5$ polaritons per site we obtain a $T_c = 4.8\text{K}$ – a temperature that is readily accessible in helium cooled setups. Surface modes can not be directly driven with a laser since their dispersion lays outside the light-cone but can instead be driven by irradiating a tip that then produces near-fields driving the modes.⁴⁶

Discussion.— We introduced a simple microscopic mechanism based on a boson coupled to an electronic interband transition which demonstrates both photo-induced enhancement of superconductivity, as well as resonant amplification of this enhancement when the phonon frequency is red-detuned but nearly aligned with the electronic excitation energy between the Fermi level in the partially filled lower band and the empty upper band. We demonstrated that this is true both using ED for a two-site model and by deriving a gap equation for extended systems.

Tantalizingly, we showed that this interaction can be

engineered in a two-dimensional material on a surface phonon polariton platform. For an example heterostructure of graphene-hBN-SrTiO₃, we computed that superconductivity can arise at temperatures around $T_c \approx 5\text{K}$.

Away from resonance the authors have studied the potential of this model to induce long-lived superconductivity.⁴⁷ This raises the compelling prospect that resonantly photo-induced superconductivity may not be only a transient phenomenon but live long after the driving has been switched off. To estimate the life-time and dynamics of the driven system, a fully non-equilibrium approach needs to be adopted so that heating, electron and phonon decoherence processes, ignored in our analysis, are taken into account on the same footing as the induced attraction.

In view of the resonant nature of our mechanism, an interesting future direction is to explore its applicability in the context of cavity material engineering^{48–52} for which several proposals for cavity-induced superconductivity already exist.^{53–57}

METHODS

Schrieffer-Wolf transformation We perform a Schrieffer-Wolf transformation of the local Hamiltonian Eq. (1) according to

$$H^{\text{SW}} = e^S H^{\text{loc}} e^{-S} \quad (16)$$

using as transformation matrix⁵⁸

$$S = \frac{\alpha}{\omega} \sum_j (b_j^\dagger - b_j) \sum_\sigma (d_{j,\sigma}^\dagger c_{j,\sigma} + c_{j,\sigma}^\dagger d_{j,\sigma}) + i \frac{\beta}{\omega} \sum_j (b_j^\dagger + b_j) \sum_\sigma (d_{j,\sigma}^\dagger c_{j,\sigma} - c_{j,\sigma}^\dagger d_{j,\sigma}). \quad (17)$$

with α and β to be determined by the condition

$$[S, H_0] = -H_{\text{int}}. \quad (18)$$

This condition is satisfied when

$$\alpha = \frac{g\omega^2}{\Delta^2 - \omega^2} \quad (19)$$

$$\beta = -i \frac{g\omega\Delta}{\Delta^2 - \omega^2}$$

The effective Schrieffer-Wolf Hamiltonian to order g^2 are calculated via $\frac{1}{2}[S, V]$ which gives rise to equation (2) in the results section.

Attractive correlations in ED.— In order to explore the resonant regime $\Omega \approx \Delta$ for the model Eq. (5) we perform ED calculations using a cutoff in the number-state basis in the bosonic part of the Hilbertspace. To explore the out of equilibrium properties we add a driving term to the Hamiltonian

$$H(t) = H + F(t) \sin(\omega_D t) \sum_j (b_j^\dagger + b_j) \quad (20)$$

where ω_D is the driving frequency and $F(t)$ has normalized Gaussian shape in time multiplied by a bare driving strength F_0 . We always drive the bosons on resonance setting $\omega_D = \Omega$. We evolve the system in time with the time evolution operator $U(t) = \mathcal{T} \exp\left(i \int_{t_0}^{t_1} H(t) dt\right)$, where \mathcal{T} is the time-ordering operator, using finite time steps. We compute the time-averaged local doublon correlations

$$\bar{C} = \int_{t_0}^{t_1} \langle n_{j,\uparrow}^c n_{j,\downarrow}^c \rangle(t) - \langle n_{j,\uparrow}^c \rangle(t) \langle n_{j,\downarrow}^c \rangle(t) dt \quad (21)$$

reported in Fig. 1b together with the time-averaged boson number. Here t_0 is a time shortly after the pump while t_1 is a later time after many driving periods.

Effective electron-electron interaction.— We use the path-integral formalism to derive a dynamic electron-electron interaction from the model Eq. (8). The bare action of the system, including bosonic modes, can be written as

$$S_0 = \sum_q \bar{b}_q D(q)^{-1} b_q + \sum_{k,\sigma,n} \bar{\psi}_{k,\sigma,n} G_0^{-1}(k,n) \psi_{k,\sigma,n} \quad (22)$$

where $k = (\vec{k}, i\omega)$ and $q = (\vec{q}, i\Omega)$ are composite indices of a lattice momentum \vec{k} or \vec{q} and a fermionic(bosonic) Matsubara frequency $\omega(\Omega)$. The b_q are complex field, \bar{b}_q their complex conjugate and $D(q)^{-1} = i\Omega - \Omega(\vec{q})$ is the inverse bosonic propagator. $\psi_{k,\sigma,n}$ and $\bar{\psi}_{k,\sigma,n}$ are Grassmann valued field with spin index $\sigma \in \{\uparrow, \downarrow\}$ and band-index $n \in \{c, d\}$ and $G_0^{-1}(k,n) = i\omega - \varepsilon_n(\vec{k})$ is the inverse bare electronic Green's function. We introduce an inter-band coupling via the bosonic fields as

$$S_{\text{int}} = \sum_q g(\vec{q}) (b_q + \bar{b}_{-q}) \left(\sum_{k,\sigma,n} \bar{\psi}_{k+q,\sigma,n} \psi_{k,\sigma,\bar{n}} \right). \quad (23)$$

Assuming a 2-band model we have introduced \bar{n} as the band complementing that labelled by the band index n . $g(\vec{q})$ is the \vec{q} dependent inter-band coupling. Now we can integrate out the bosons with a suitable substitution of the bosonic fields in the path integral to arrive at an effective interaction

$$S_{\text{int}}^{\text{eff}} = - \sum_q g(\vec{q}) g(-\vec{q}) D(q) \left(\sum_{k,\sigma,n} \bar{\psi}_{k+q,\sigma,n} \psi_{k,\sigma,\bar{n}} \right) \left(\sum_{k',\sigma',m} \bar{\psi}_{k'-q,\sigma',m} \psi_{k',\sigma',\bar{m}} \right). \quad (24)$$

Due to the sum over q and since all other terms are even in q one may perform the replacement

$$D(q) \rightarrow \frac{-\Omega(\vec{q})}{\Omega^2 + \Omega(\vec{q})^2} \quad (25)$$

taking only the part of the propagator even in q . Equations (9) and (10) are derived using the saddle point

approximation in the Cooper channel, leading to a self-consistent equation shown schematically in Fig. 2(a). A key aspect of our work is performing the Matsubara sums analytically and expressing the result in terms of occupation distributions of the bosons and fermions. In the main text we show an approximate formula of the most divergent terms, for completeness we report here the full

gap equation. We take the full ω and k dependence of Δ_d by replacing the expression for Δ_d in equation (10) into equation (9), to arrive at a self-consistent equation for Δ_c only. We then find that the expression for Δ_c is weakly frequency dependent for $\omega \ll \Omega$ which allows to approximate Δ_c as independent of ω and k . The resulting gap equation is found to be:

$$\begin{aligned}
1 = & \frac{1}{N^2} \sum_{k',k} |g|^4 \frac{1}{E_1(k)E_2(k')} \times \left(\frac{(2n_f(E_1) - 1)(E_1(k)^2(2E_2(k')n_b(\Omega) + E_2(k') - 2n_f(E_2)\Omega + \Omega))}{\Omega(\Omega^2 - E_1(k)^2)((E_2(k') - \Omega)^2 - E_1(k)^2)((E_2(k') + \Omega)^2 - E_1(k)^2)} + \right. \\
& \left. \frac{(2n_f(E_1) - 1)((\Omega - E_2(k'))(E_2(k') + \Omega)(2E_2(k')n_b(\Omega) + E_2(k') + (2n_f(E_2) - 1)\Omega))}{\Omega(\Omega^2 - E_1(k)^2)((E_2(k') - \Omega)^2 - E_1(k)^2)((E_2(k') + \Omega)^2 - E_1(k)^2)} \right) \\
& + \frac{4E_1(k)E_2(k')(n_f(\Omega + E_2(k')) - 1)(E_2(k') + \Omega)(n_b(\Omega) - n_f(E_2) + 1)}{-4E_2(k')^2\Omega(E_2(k') + \Omega)(E_2(k') + 2\Omega)((E_2(k') + \Omega)^2 - E_1(k)^2)} \\
& + \frac{4E_1(k)E_2(k')(n_f(\Omega - E_2(k')) - 1)(E_2(k') - \Omega)(n_b(\Omega) + n_f(E_2))}{4E_2(k')^2\Omega(E_2(k') - 2\Omega)(E_2(k') - \Omega)((E_2(k') - \Omega)^2 - E_1(k)^2)} \\
& + \frac{-4E_1(k)E_2(k')n_f(\Omega - E_2(k'))(E_2(k') - \Omega)(n_b(\Omega) + n_f(E_2))}{-4E_2(k')^2\Omega(E_2(k') - 2\Omega)(E_2(k') - \Omega)((E_2(k') - \Omega)^2 - E_1(k)^2)} \\
& + \frac{4E_1(k)E_2(k')n_f(\Omega + E_2(k'))(E_2(k') + \Omega)(n_b(\Omega) - n_f(E_2) + 1)}{-4E_2(k')^2\Omega(E_2(k') + \Omega)(E_2(k') + 2\Omega)((E_2(k') + \Omega)^2 - E_1(k)^2)} \\
& + \frac{E_1(k)E_2(k')(n_b(\Omega) + 1)(E_2(k')^2(2n_b(\Omega) + 1) + E_2(k')(2n_f(E_2) - 1)\Omega - 2(2n_b(\Omega) + 1)\Omega^2)}{\Omega^2(E_1(k)^2 - \Omega^2)(E_2(k')^4 - 4E_2(k')^2\Omega^2)} \\
& \left. \frac{E_1(k)E_2(k')n_b(\Omega)(E_2(k')^2(2n_b(\Omega) + 1) + E_2(k')(2n_f(E_2) - 1)\Omega - 2(2n_b(\Omega) + 1)\Omega^2)}{\Omega^2(E_1(k)^2 - \Omega^2)(E_2(k')^4 - 4E_2(k')^2\Omega^2)} \right) \quad (26)
\end{aligned}$$

Graphene coupled to surface phonon polaritons. – In this part we outline the estimate of the pairing temperature of our proposed heterostructure consisting of Graphene aligned with hBN on top of bulk SrTiO₃. We use the q -dependent surface phonon-polariton modes given in Ref. 43 that read

$$\begin{aligned}
\phi(z > 0) = & N \left(\frac{q_x}{|q_{xy}|}, \frac{q_y}{|q_{xy}|}, i \sqrt{\left| \frac{\varepsilon(\omega)}{\varepsilon_{\text{hBN}}} \right|} \right)^T \\
& e^{-\sqrt{\left| \frac{\varepsilon_{\text{hBN}}}{\varepsilon(\omega)} \right|} |q_{xy}|z} e^{i(q_x x + q_y y - \omega t)} \quad (27) \\
\phi(z < 0) = & N \left(\frac{q_x}{|q_{xy}|}, \frac{q_y}{|q_{xy}|}, -i \sqrt{\left| \frac{\varepsilon_{\text{hBN}}}{\varepsilon(\omega)} \right|} \right)^T \\
& e^{\sqrt{\left| \frac{\varepsilon(\omega)}{\varepsilon_{\text{hBN}}} \right|} |q_{xy}|z} e^{i(q_x x + q_y y - \omega t)}
\end{aligned}$$

where the upper half-space $z > 0$ is assumed to be filled with hBN with dielectric constant $\varepsilon_{\text{hBN}} = 5^{59}$ while the lower half-space is made up of the SrTiO₃ with $\varepsilon(\omega) = \varepsilon_\infty \frac{\omega_{\text{LO}}^2 - \omega^2}{\omega_{\text{TO}}^2 - \omega^2}$. We use $\varepsilon_\infty = 6.3^{60}$, $\omega_{\text{TO}} = 1.26\text{THz}$ and $\omega_{\text{LO}} = 5.1\text{THz}$.⁶¹ The normalization N of the modes can

be determined from the normalization condition⁴³

$$\hbar\Omega_s \varepsilon_0 \int_V dr \varepsilon(\Omega_s) v(\Omega_s) |\phi(r)|^2 = 1. \quad (28)$$

with $v(\omega) = 2 + \omega \partial_\omega \varepsilon(\omega)$ and ε_0 the vacuum permittivity. The limiting surface phonon frequency when $c^2 q^2 \ll \omega_{\text{LO}}^2$ is $\Omega_s = 3.9\text{THz}$ which we will use throughout for our estimate. In order to estimate the light-matter coupling we focus on the Dirac cone at which the Hamiltonian, including the gap opening due to an effective onsite potential induced through the proximity of hBN to the graphene layer, reads

$$H = \frac{V_0}{2} \sigma_z + \hbar v_F (k + eA) \cdot \sigma. \quad (29)$$

where V_0 is the onsite potential, v_F the Fermi velocity and A the vector potential due to the surface polaritons. At the K -point the inter-band coupling is equal to $g_{\text{inter}} = 1$ while far away from the K -point it can be estimated from the Dirac Hamiltonian without including an onsite potential which yields $g_{\text{inter}} = \frac{i\hbar v_F (k \times A)}{|k|}$. Using the coupling away from the K -point as a conservative

estimate, we get for the inter-band coupling

$$g^{k,q} = i \frac{\sqrt{4\pi\alpha}}{\sqrt{N}} f(\omega) \frac{\hbar v_F \sqrt{c}}{\sqrt{\Omega_s S_{\text{cell}}}} \frac{(k \times q)}{|q||k|} \sqrt{|q_{xy}|} e^{-|q_{xy}|z} \quad (30)$$

where $f(\omega) = \left(4 \frac{\omega^2(\varepsilon_\infty + \varepsilon_{\text{HBN}})}{\omega^2 - \omega_{\text{TO}}^2}\right)^{-\frac{1}{2}}$, S_{cell} is the area of the unit cell in graphene, α the fine-structure constant and c the speed of light. In order to obtain a simple estimate we approximate the coupling by a box function $g^{k,q} \rightarrow \tilde{g}\theta(|q| - \frac{1}{d})$. The cutoff $\frac{1}{d}$ is naturally provided by the mode-function Eq. (27) since $\varepsilon(\omega) \rightarrow -\varepsilon_{\text{HBN}}$ for $q^2 c^2 \ll \omega_{\text{LO}}^2$ and therefore $|\theta(q)|^2 \sim e^{-2qd}$. We determine \tilde{g} by fixing the integral

$$\tilde{g}^2 = \int_{\mathbb{R}^2} |g^{k,q}|^2 dq = \frac{2\pi\alpha}{3\sqrt{3}N} f(\omega)^2 \frac{\hbar^2 v_F^2 c}{a^2 d} \quad (31)$$

where we use g^2 since this appears in the interaction. Due to the box-function the coupling has now attained a q dependence in principle leading to a k -dependence of the gap itself. We compute the gap at $k = K$ and assume it to be zero outside of the coupling radius $\theta(k)$. Additionally, the momentum transfer $k - k'$ is limited due to the box coupling by a factor $\theta(k - k')$. We set the chemical potential $\mu = -15\text{meV}$ slightly into the lower band and otherwise the parameters from the main text. With these approximations we are in a position to evaluate Eq. (26) on a finite k -grid for which we use the size 500×500 . For the driven case we assume a non-thermal boson occupation according to Eq. (15).

-
- [1] Basov, D. N., Averitt, R. D. & Hsieh, D. Towards properties on demand in quantum materials. *Nature Mater* **16**, 1077–1088 (2017). URL <https://www.nature.com/articles/nmat5017>. Number: 11 Publisher: Nature Publishing Group.
- [2] de la Torre, A. *et al.* Colloquium: Nonthermal pathways to ultrafast control in quantum materials. *Rev. Mod. Phys.* **93**, 041002 (2021). URL <https://link.aps.org/doi/10.1103/RevModPhys.93.041002>. Publisher: American Physical Society.
- [3] Disa, A. S., Nova, T. F. & Cavalleri, A. Engineering crystal structures with light. *Nat. Phys.* **17**, 1087–1092 (2021). URL <https://www.nature.com/articles/s41567-021-01366-1>. Number: 10 Publisher: Nature Publishing Group.
- [4] Nova, T. F., Disa, A. S., Fechner, M. & Cavalleri, A. Metastable ferroelectricity in optically strained SrTiO₃. *Science* **364**, 1075–1079 (2019). URL <https://www.science.org/doi/10.1126/science.aaw4911>. Publisher: American Association for the Advancement of Science.
- [5] Li, X. *et al.* Terahertz field-induced ferroelectricity in quantum paraelectric SrTiO₃. *Science* **364**, 1079–1082 (2019). URL <https://www.science.org/doi/10.1126/science.aaw4913>. Publisher: American Association for the Advancement of Science.
- [6] Kogar, A. *et al.* Light-induced charge density wave in LaTe₃. *Nat. Phys.* **16**, 159–163 (2020). URL <https://www.nature.com/articles/s41567-019-0705-3>. Number: 2 Publisher: Nature Publishing Group.
- [7] Wandel, S. *et al.* Enhanced charge density wave coherence in a light-quenched, high-temperature superconductor. *Science* **376**, 860–864 (2022). URL <https://www.science.org/doi/10.1126/science.abd7213>. Publisher: American Association for the Advancement of Science.
- [8] Dolgirev, P. E., Michael, M. H., Zong, A., Gedik, N. & Demler, E. Self-similar dynamics of order parameter fluctuations in pump-probe experiments. *Phys. Rev. B* **101**, 174306 (2020). URL <https://link.aps.org/doi/10.1103/PhysRevB.101.174306>. Publisher: American Physical Society.
- [9] Mitrano, M. *et al.* Possible light-induced superconductivity in K3C60 at high temperature. *Nature* **530**, 461–464 (2016). URL <https://www.nature.com/articles/nature16522>. Number: 7591 Publisher: Nature Publishing Group.
- [10] Cantaluppi, A. *et al.* Pressure tuning of light-induced superconductivity in K3C60. *Nature Phys* **14**, 837–841 (2018). URL <https://www.nature.com/articles/s41567-018-0134-8>. Number: 8 Publisher: Nature Publishing Group.
- [11] Rowe, E. *et al.* Giant resonant enhancement for photo-induced superconductivity in K₃C₆₀ (2023). URL <http://arxiv.org/abs/2301.08633>. ArXiv:2301.08633 [cond-mat].
- [12] Buzzi, M. *et al.* Photomolecular High-Temperature Superconductivity. *Phys. Rev. X* **10**, 031028 (2020). URL <https://link.aps.org/doi/10.1103/PhysRevX.10.031028>. Publisher: American Physical Society.
- [13] Kennes, D. M., Wilner, E. Y., Reichman, D. R. & Millis, A. J. Transient superconductivity from electronic squeezing of optically pumped phonons. *Nature Phys* **13**, 479–483 (2017). URL <https://www.nature.com/articles/nphys4024>. Number: 5 Publisher: Nature Publishing Group.
- [14] Babadi, M., Knap, M., Martin, I., Refael, G. & Demler, E. Theory of parametrically amplified electron-phonon superconductivity. *Phys. Rev. B* **96**, 014512 (2017). URL <https://link.aps.org/doi/10.1103/PhysRevB.96.014512>. Publisher: American Physical Society.
- [15] Dolgirev, P. E. *et al.* Periodic dynamics in superconductors induced by an impulsive optical quench. *Commun Phys* **5**, 1–9 (2022). URL <https://www.nature.com/articles/s42005-022-01007-w>. Number: 1 Publisher: Nature Publishing Group.
- [16] Murakami, Y., Tsuji, N., Eckstein, M. & Werner, P. Nonequilibrium steady states and transient dynamics of conventional superconductors under phonon driving. *Phys. Rev. B* **96**, 045125 (2017). URL <https://link.aps.org/doi/10.1103/PhysRevB.96.045125>. Publisher: American Physical Society.
- [17] Sentef, M. A., Kemper, A. F., Georges, A. & Kollath, C. Theory of light-enhanced phonon-mediated superconductivity. *Phys. Rev. B* **93**, 144506 (2016). URL <https://link.aps.org/doi/10.1103/PhysRevB.93.144506>. Publisher: American Physical Society.

- [18] Michael, M. H. *et al.* Parametric resonance of Josephson plasma waves: A theory for optically amplified interlayer superconductivity in $\text{YBa}_2\text{Cu}_3\text{O}_{6+x}$. *Phys. Rev. B* **102**, 174505 (2020). URL <https://link.aps.org/doi/10.1103/PhysRevB.102.174505>. Publisher: American Physical Society.
- [19] Kim, M. *et al.* Enhancing superconductivity in A_3C_{60} fullerides. *Phys. Rev. B* **94**, 155152 (2016). URL <https://link.aps.org/doi/10.1103/PhysRevB.94.155152>. Publisher: American Physical Society.
- [20] Mazza, G. & Georges, A. Nonequilibrium superconductivity in driven alkali-doped fullerides. *Phys. Rev. B* **96**, 064515 (2017). URL <https://link.aps.org/doi/10.1103/PhysRevB.96.064515>. Publisher: American Physical Society.
- [21] Nava, A., Giannetti, C., Georges, A., Tosatti, E. & Fabrizio, M. Cooling quasiparticles in A_3C_{60} fullerides by excitonic mid-infrared absorption. *Nat. Phys.* **14**, 154–159 (2018). URL <https://www.nature.com/articles/nphys4288>. Number: 2 Publisher: Nature Publishing Group.
- [22] Denny, S., Clark, S., Laplace, Y., Cavalleri, A. & Jaksch, D. Proposed Parametric Cooling of Bilayer Cuprate Superconductors by Terahertz Excitation. *Phys. Rev. Lett.* **114**, 137001 (2015). URL <https://link.aps.org/doi/10.1103/PhysRevLett.114.137001>. Publisher: American Physical Society.
- [23] Dasari, N. & Eckstein, M. Transient Floquet engineering of superconductivity. *Phys. Rev. B* **98**, 235149 (2018). URL <https://link.aps.org/doi/10.1103/PhysRevB.98.235149>. Publisher: American Physical Society.
- [24] Sentef, M. A. Light-enhanced electron-phonon coupling from nonlinear electron-phonon coupling. *Phys. Rev. B* **95**, 205111 (2017). URL <https://link.aps.org/doi/10.1103/PhysRevB.95.205111>. Publisher: American Physical Society.
- [25] Murakami, Y., Werner, P., Tsuji, N. & Aoki, H. Interaction quench in the Holstein model: Thermalization crossover from electron- to phonon-dominated relaxation. *Phys. Rev. B* **91**, 045128 (2015). URL <https://link.aps.org/doi/10.1103/PhysRevB.91.045128>. Publisher: American Physical Society.
- [26] Coulthard, J. R., Clark, S. R., Al-Assam, S., Cavalleri, A. & Jaksch, D. Enhancement of superexchange pairing in the periodically driven Hubbard model. *Phys. Rev. B* **96**, 085104 (2017). URL <https://link.aps.org/doi/10.1103/PhysRevB.96.085104>. Publisher: American Physical Society.
- [27] Okamoto, J.-i., Cavalleri, A. & Mathey, L. Theory of Enhanced Interlayer Tunneling in Optically Driven High- T_c Superconductors. *Phys. Rev. Lett.* **117**, 227001 (2016). URL <https://link.aps.org/doi/10.1103/PhysRevLett.117.227001>. Publisher: American Physical Society.
- [28] Komnik, A. & Thorwart, M. BCS theory of driven superconductivity. *Eur. Phys. J. B* **89**, 244 (2016). URL <https://doi.org/10.1140/epjb/e2016-70528-1>.
- [29] Knap, M., Babadi, M., Refael, G., Martin, I. & Demler, E. Dynamical Cooper pairing in nonequilibrium electron-phonon systems. *Phys. Rev. B* **94**, 214504 (2016). URL <https://link.aps.org/doi/10.1103/PhysRevB.94.214504>. Publisher: American Physical Society.
- [30] Raines, Z. M., Stanev, V. & Galitski, V. M. Enhancement of superconductivity via periodic modulation in a three-dimensional model of cuprates. *Phys. Rev. B* **91**, 184506 (2015). URL <https://link.aps.org/doi/10.1103/PhysRevB.91.184506>. Publisher: American Physical Society.
- [31] Dai, Z. & Lee, P. A. Superconducting-like response in driven systems near the Mott transition. *Phys. Rev. B* **104**, L241112 (2021). URL <https://link.aps.org/doi/10.1103/PhysRevB.104.L241112>. Publisher: American Physical Society.
- [32] Ngai, K. L. Two-Phonon Deformation Potential and Superconductivity in Degenerate Semiconductors. *Phys. Rev. Lett.* **32**, 215–218 (1974). URL <https://link.aps.org/doi/10.1103/PhysRevLett.32.215>. Publisher: American Physical Society.
- [33] Enaki, N. A. & Ereameev, V. V. Cooperative two-phonon phenomena in superconductivity. *New J. Phys.* **4**, 80 (2002). URL <https://dx.doi.org/10.1088/1367-2630/4/1/380>.
- [34] Kiselov, D. E. & Feigel'man, M. V. Theory of superconductivity due to Ngai's mechanism in lightly doped SrTiO_3 . *Phys. Rev. B* **104**, L220506 (2021). URL <https://link.aps.org/doi/10.1103/PhysRevB.104.L220506>. Publisher: American Physical Society.
- [35] Slotman, G. *et al.* Effect of Structural Relaxation on the Electronic Structure of Graphene on Hexagonal Boron Nitride. *Phys. Rev. Lett.* **115**, 186801 (2015). URL <https://link.aps.org/doi/10.1103/PhysRevLett.115.186801>. Publisher: American Physical Society.
- [36] Xue, J. *et al.* Scanning tunnelling microscopy and spectroscopy of ultra-flat graphene on hexagonal boron nitride. *Nature Mater* **10**, 282–285 (2011). URL <https://www.nature.com/articles/nmat2968>. Number: 4 Publisher: Nature Publishing Group.
- [37] Yankowitz, M. *et al.* Emergence of superlattice Dirac points in graphene on hexagonal boron nitride. *Nature Phys* **8**, 382–386 (2012). URL <https://www.nature.com/articles/nphys2272>. Number: 5 Publisher: Nature Publishing Group.
- [38] Dean, C. *et al.* Graphene based heterostructures. *Solid State Communications* **152**, 1275–1282 (2012). URL <https://www.sciencedirect.com/science/article/pii/S003810981200227X>.
- [39] Huber, S. D. & Altman, E. Bose condensation in flat bands. *Phys. Rev. B* **82**, 184502 (2010). URL <https://link.aps.org/doi/10.1103/PhysRevB.82.184502>. Publisher: American Physical Society.
- [40] Zhang, T. & Jo, G.-B. One-dimensional sawtooth and zigzag lattices for ultracold atoms. *Sci Rep* **5**, 16044 (2015). URL <https://www.nature.com/articles/srep16044>. Number: 1 Publisher: Nature Publishing Group.
- [41] Han, T. *et al.* Accurate Measurement of the Gap of Graphene-BN Moiré Superlattice through Photocurrent Spectroscopy. *Phys. Rev. Lett.* **126**, 146402 (2021). URL <https://link.aps.org/doi/10.1103/PhysRevLett.126.146402>. Publisher: American Physical Society.
- [42] Lenk, K., Li, J., Werner, P. & Eckstein, M. Dynamical mean-field study of a photon-mediated ferro-

- electric phase transition. *Phys. Rev. B* **106**, 245124 (2022). URL <https://link.aps.org/doi/10.1103/PhysRevB.106.245124>. Publisher: American Physical Society.
- [43] Gubbin, C. R., Maier, S. A. & De Liberato, S. Real-space Hopfield diagonalization of inhomogeneous dispersive media. *Phys. Rev. B* **94**, 205301 (2016). URL <https://link.aps.org/doi/10.1103/PhysRevB.94.205301>. Publisher: American Physical Society.
- [44] Golla, D. *et al.* Optical thickness determination of hexagonal boron nitride flakes. *Applied Physics Letters* **102**, 161906 (2013). URL <https://aip.scitation.org/doi/abs/10.1063/1.4803041>. Publisher: American Institute of PhysicsAIP.
- [45] Morel, P. & Anderson, P. W. Calculation of the Superconducting State Parameters with Retarded Electron-Phonon Interaction. *Phys. Rev.* **125**, 1263–1271 (1962). URL <https://link.aps.org/doi/10.1103/PhysRev.125.1263>. Publisher: American Physical Society.
- [46] Basov, D. N., Fogler, M. M. & García de Abajo, F. J. Polaritons in van der Waals materials. *Science* **354**, aag1992 (2016). URL <https://www.science.org/doi/10.1126/science.aag1992>. Publisher: American Association for the Advancement of Science.
- [47] Chattopadhyay, S. *et al.* Mechanisms for Long-Lived, Light-Induced Superconductivity, far above T_c (2023).
- [48] Schlawin, F., Kennes, D. M. & Sentef, M. A. Cavity quantum materials. *Applied Physics Reviews* **9**, 011312 (2022). URL <https://aip.scitation.org/doi/10.1063/5.0083825>. Publisher: American Institute of Physics.
- [49] Bloch, J., Cavalleri, A., Galitski, V., Hafezi, M. & Rubio, A. Strongly correlated electron–photon systems. *Nature* **606**, 41–48 (2022). URL <https://www.nature.com/articles/s41586-022-04726-w>. Number: 7912 Publisher: Nature Publishing Group.
- [50] Ruggenthaler, M., Tancogne-Dejean, N., Flick, J., Appel, H. & Rubio, A. From a quantum-electrodynamical light–matter description to novel spectroscopies. *Nat Rev Chem* **2**, 1–16 (2018). URL <https://www.nature.com/articles/s41570-018-0118>. Number: 3 Publisher: Nature Publishing Group.
- [51] Frisk Kockum, A., Miranowicz, A., De Liberato, S., Savasta, S. & Nori, F. Ultrastrong coupling between light and matter. *Nat Rev Phys* **1**, 19–40 (2019). URL <https://www.nature.com/articles/s42254-018-0006-2>. Number: 1 Publisher: Nature Publishing Group.
- [52] Hübener, H. *et al.* Engineering quantum materials with chiral optical cavities. *Nat. Mater.* **20**, 438–442 (2021). URL <https://www.nature.com/articles/s41563-020-00801-7>. Number: 4 Publisher: Nature Publishing Group.
- [53] Andolina, G. M. *et al.* Can deep sub-wavelength cavities induce Amperean superconductivity in a 2D material? (2022). URL <http://arxiv.org/abs/2210.10371>. ArXiv:2210.10371 [cond-mat].
- [54] Schlawin, F., Cavalleri, A. & Jaksch, D. Cavity-Mediated Electron-Photon Superconductivity. *Phys. Rev. Lett.* **122**, 133602 (2019). URL <https://link.aps.org/doi/10.1103/PhysRevLett.122.133602>. Publisher: American Physical Society.
- [55] Gao, H., Schlawin, F., Buzzzi, M., Cavalleri, A. & Jaksch, D. Photo-induced electron pairing in a driven cavity. *Phys. Rev. Lett.* **125**, 053602 (2020). URL <http://arxiv.org/abs/2003.05319>. ArXiv:2003.05319 [cond-mat].
- [56] Chakraborty, A. & Piazza, F. Long-Range Photon Fluctuations Enhance Photon-Mediated Electron Pairing and Superconductivity. *Phys. Rev. Lett.* **127**, 177002 (2021). URL <https://link.aps.org/doi/10.1103/PhysRevLett.127.177002>. Publisher: American Physical Society.
- [57] Dé, B. L., Eckhardt, C. J., Kennes, D. M. & Sentef, M. A. Cavity engineering of Hubbard U via phonon polaritons. *J. Phys. Mater.* **5**, 024006 (2022). URL <http://arxiv.org/abs/2201.04128>. ArXiv:2201.04128 [cond-mat, physics:physics].
- [58] Michael, M. *et al.* Fresnel-Floquet theory of light-induced terahertz reflectivity amplification in Ta₂NiSe₅ (2022). URL <http://arxiv.org/abs/2207.08851>. ArXiv:2207.08851 [cond-mat, physics:quant-ph].
- [59] Cai, Y., Zhang, L., Zeng, Q., Cheng, L. & Xu, Y. Infrared reflectance spectrum of BN calculated from first principles. *Solid State Communications* **141**, 262–266 (2007). URL <https://www.sciencedirect.com/science/article/pii/S0038109806009719>.
- [60] van Roekeghem, A., Carrete, J., Curtarolo, S. & Mingo, N. High-throughput study of the static dielectric constant at high temperatures in oxide and fluoride cubic perovskites. *Phys. Rev. Mater.* **4**, 113804 (2020). URL <https://link.aps.org/doi/10.1103/PhysRevMaterials.4.113804>. Publisher: American Physical Society.
- [61] Evarestov, R. A., Blokhin, E., Gryaznov, D., Kotomin, E. A. & Maier, J. Phonon calculations in cubic and tetragonal phases of SrTiO₃: A comparative LCAO and plane-wave study. *Phys. Rev. B* **83**, 134108 (2011). URL <https://link.aps.org/doi/10.1103/PhysRevB.83.134108>. Publisher: American Physical Society.